ACS APPLIED MATERIALS & INTERFACES

Research Article

www.acsami.org

Morphological Evolution of Gyroid-Forming Block Copolymer Thin Films with Varying Solvent Evaporation Rate

Yi-Hsiu Wu, Ting-Ya Lo, Ming-Shiuan She, and Rong-Ming Ho*

Department of Chemical Engineering, National Tsing Hua University, Hsinchu 30013, Taiwan Republic of China

Supporting Information

ABSTRACT: In this study, we aim to examine the morphological evolution of block copolymer (BCP) nanostructured thin films through solvent evaporation at different rates for solvent swollen polystyrene-*block*-poly(L-lactide) (PS−PLLA). Interesting phase transitions from disorder to perpendicular cylinder and then gyroid can be found while using a partially selective solvent for PS to swell PS−PLLA thin film followed by solvent evaporation. During the transitions, gyroid-forming BCP thin film with characteristic crystallographic planes of $(111)_G$, $(110)_G$, and $(211)_G$ parallel to air surface can be observed, and will gradually transform into coexisting $(110)_G$ and $(211)_G$ planes, and finally transforms to $(211)_G$ plane due to the preferential segregation of constituted block to the surface (i.e., the thermodynamic origin for self-assembly) that affects the relative amount of each component at the air surface. With the decrease on the evaporation rate, the disorder phase will transform to parallel cylinder and then directly to $(211)_G$ without transition to perpendicular cylinder phase. Most importantly, the morphological evolution of PS−PLLA thin films is strongly dependent upon the solvent removal rate only in the initial stage of the evaporation process due to the anisotropy of cylinder structure. Once the morphology is transformed back to the isotropic gyroid structure after long evaporation, the morphological evolution will only relate to the variation of the surface composition. Similar phase transitions at the substrate can also be obtained by controlling the ratio of PLLA−OH to PS−OH homopolymers to functionalize the substrate. As a result, the fabrication of well-defined nanostructured thin films with controlled orientation can be achieved by simple swelling and deswelling with controlled evaporation rate.

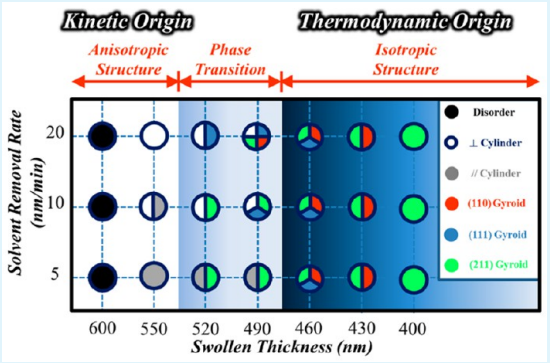

KEYWORDS: *solvent evaporation, solvent annealing, thin films, block copolymers, ordering, gyroid*

INTRODUCTION

Nanostructured thin films from the self-assembly of block copolymers (BCPs) have drawn intensive attention due to their appealing applications in templates,[1−3] membranes,[4−8] antireflection coatings,[9,10] nanolithography,[11] and optoelectronics.[12] For the ordering of BCP thin films, the self-assembled morphologies are strongly affected by commensurability (the ratio of film thickness to domain spacing) and interfacial interactions (the interactions of constituted blocks with the air and substrate) in addition to interaction parameter, molecular weight, and composition.[13,14] A variety of ordered nanostructures, such as body-center cubic spheres, hexagonally packed cylinders, double gyroid, and lamellae, can be obtained from the self-assembly of BCPs in the thin-film state. Among them, double gyroid is one of the most appealing morphologies for practical applications because of its unique texture, composed of a matrix and two continuous but independent, interpenetrating networks in three-dimensional space, giving well-defined network morphology.[15−18] Different approaches to control the ordering of BCP thin films have been reported.[19−27] The use of solvent field (that is, solvent annealing or solvent evaporation) is an alternative method for ordering BCP thin films because BCPs encounters severe thermal degradation after high temperature thermal treatment.[28−32] The absorption of solvent promotes the self-assembly of BCP thin films by lowering the glass transition temperature of constituted blocks to give sufficient chain mobility for ordering. The selectivity of the solvent vapor can create an effectively neutral air surface or a surface that preferentially attracts the block with high surface tension by reducing preferential segregation of the block with low surface tension to the free surface, giving controlled orientation of BCP nanostructure from ordering. After the treatment in solvent field, instantaneous solvent removal is usually employed to trap the morphologies from the solvent-swollen thin films. Moreover, the absorption of selective solvent may result in the variation of effective volume fraction of the constituted block and thus microphase-separated nanostructured phase that enriches the applications of BCP self-assembly.

Libera and co-workers[19] are the first to demonstrate the effect of solvent evaporation on the orientation of cylinder microdomains normal to the film surfaces of different BCP thin films. In our previous studies, the preparation of perpendicular

Received: May 9, 2015
Accepted: July 7, 2015
Published: July 7, 2015

DOI: 10.1021/acsami.5b03977
ACS Appl. Mater. Interfaces 2015, 7, 16536−16547

poly(L-lactide) (PLLA) cylinders in polystyrene-*block*-poly(L-lactide) (PS−PLLA) thin film can be achieved by controlling the evaporation rate and the selectivity of the solvent with constituted blocks of the PS−PLLA.[27] In addition to control of the orientation of cylinders, the long-range order of the cylinders in BCP thin films is also important for applications. Among several plausible routes, annealing in solvent vapor has been shown to be effective in enhancing the lateral order of BCP thin films over large areas.[28−32] Russell and co-workers investigated the thin-film morphologies of polystyrene-*b*-poly(ethylene oxide) (PS−PEO) and polystyrene-*b*-poly(4-vinylpyridine) (PS-P4VP) after annealing in solvent vapor.[28,29] With increasing the annealing time, the lateral ordering of the cylinders can be significantly enhanced, giving BCP thin films with a hexagonal ordering of the cylinders. Recently, Epps and co-workers reported a systematic studies on induced cylinder orientation in BCP thin films through the control of solvent evaporation rate for swollen thin films by solvent.[31] In our previous study, the morphological evolution for the gyroid-forming block copolymer thin films was studied as a function of solvent annealing time by keeping the swollen thickness at two times of the initial thickness. When the solvent annealing of the gyroid-forming PS−PLLA thin film was keep at a certain swollen thickness for a sufficiently long time, interesting morphological evolution from gyroid to cylinder can be found.[32] Furthermore, the thin film morphologies at the free surface will be strongly affected by solvent evaporation rate, whereas the morphologies at the interface of the film and substrate were dependent on the interactions of constituted blocks with the substrate. With the use of neutral substrates, the formation of perpendicular cylinders in BCP thin films can be achieved. In literature, numerous methods have been reported for the fabrication of neutral substrates.[33−44] Recently, we also demonstrated a new method for the formation of well-defined nanostructured thin films with the aid of a two-step surface functionalization.[44]

Herein, we aim to systematically investigate the effect of solvent evaporation rate on the ordering of solvent-swollen gyroid-forming PS−PLLA thin film. To gain insight into the reordering mechanism associated with removal of solvent, the as-cast BCP thin films will be swollen to reach disordered state (swollen to 3 times the initial thickness), and then morphological evolution can be induced by controlling the rate of solvent evaporation. The thin-film morphologies will be kinetically trapped at different preset time points during solvent evaporation by instantaneous removal of the solvent. In particular, the effects of the initial stage on the following solvent annealing and evaporation processes will be emphasized. As mentioned above, the swollen thickness studied in our previous report is 2 times the initial thickness;[32] therefore, the morphological evolution is initiated from the microphase-separated condition in that case. By contrast, the ordering process in this study is initiated from the disordered state during the solvent evaporation with controlled evaporation rate at which the thickness will be varied during solvent evaporation. Interesting morphological transformation behaviors from disordered state to parallel cylinder, perpendicular cylinder, and finally to gyroid can be found by using a partially PS selective solvent to anneal the PS−PLLA thin film (note that the use of PLLA selective solvents and neutral solvents will encounter the crystallization problem during swelling of the thin film, eventually resulting in the disturbance of well-developed nanostructured thin film). The orientation of the gyroid morphology was further studied by computational calculation of compositional fraction, suggesting that the forming thin-film morphologies can be dominated by thermodynamic origin once the evaporation rate is low enough to annihilate the kinetic effect on BCP self-assembly. Meanwhile, to alleviate the wetting problem of the PS near the substrate, the preferentiality of functionalized SiO_2 substrate is tuned by increasing the proportion of the grafted PLLA−OH to balance the selectivity of the substrate upon solvent evaporation. Consequently, the formation of well-ordered gyroid-forming PS−PLLA thin film with uniform surface and open-cell character can be achieved and used for various applications in nanotechnologies. Furthermore, well-ordered nanoporous polymers can be fabricated after removal of the PLLA block in the self-assembled PS−PLLA gyroid thin-film and used as polymeric templates for the synthesis of a variety of nanohybrid and nanoporous inorganic materials.[10,45−49]

EXPERIMENTAL SECTION

Materials. Hydroxyl-terminated polystyrene (PS−OH) with M_n = 10 800 g mol^{-1} and polydispersity ($Đ$) = 1.25 was synthesized by atom transfer radical polymerization (ATRP). Hydroxyl-terminated poly(L-lactide) (PLLA−OH) with M_n = 10 500 g mol^{-1} and $Đ$ = 1.16 was synthesized by ring-opening polymerization (ROP). The PS−PLLA was prepared by a sequential living polymerization using a double-headed initiator. The synthetic routes of the PS−PLLA sample were described in our previous publication.[10,45−49] The number-average molecular weight and the $Đ$ of the PS block were determined by gel permeation chromatography (GPC). The $Đ$ of the PS−PLLA was determined by GPC, and the number of L-LA repeating units was determined as a function of the number of styrene repeating units by ^{1}H NMR analysis. The self-assembled PS−PLLA in the bulk state used in this study is a gyroid phase, as reported previously.[10,45−49] The domain spacing of the $(211)_G$ plane and lattice constant of the gyroid phase were determined as approximately 40.9 and 100.1 nm, respectively, on the basis of small-angle X-ray scattering (SAXS) results.[12] The number-average molecular weights of the PS and PLLA blocks were 34 000 g mol^{-1} and 27 000 g mol^{-1}, respectively, and the $Đ$ of the PS−PLLA was 1.26. The volume fraction of PLLA was calculated to be f_{PLLA}^{ν} = 0.39 by assuming that the densities of the PS and the PLLA were 1.02 and 1.25 gcm^{-3}, respectively. Silicon (Si) substrate was cleaned using a piranha solution (30:70 v/v% of H_2O_2 /H_2SO_4) at 140 °C for 30 min, followed by rinsing with deionized water and drying in flowing nitrogen gas.

Preparation of Functionalized SiO_2 with Mixed Homopolymer Brushes. Following the procedures described in our previous study,[44] we successfully prepared functionalized SiO_2 with mixed homopolymer brushes. The polymer solution (1 wt % PS−OH) in 1,2-dichloroethane was spin-coated onto Si wafer with SiO_2 surface at 1000 rpm for 1 min. Subsequently, the Si wafer with SiO_2 surface coated with a thin layer of PS−OH was annealed at 140 °C in a vacuum oven for different periods to graft the PS−OH onto the wafer. The treated samples were then rinsed with 1,2-dichloroethane to remove ungrafted PS−OH. Subsequently, the PLLA−OH was spin-coated on the functionalized SiO_2 with PS−OH brushes, and the film was thermally annealed at 180 °C in a vacuum oven. Finally, functionalized SiO_2 with mixed homopolymer brushes was obtained after rinsing with 1,2-dichloroethane to remove ungrafted PLLA−OH.

Preparation of Thin-Film Samples. Thin-film samples with thickness of 200 nm was prepared on the functionalized SiO_2 by spin-coating at 1000 rpm for 1 min by using 3 wt % of PS−PLLA solution in chlorobenzene and then annealed with chloroform vapor using a homemade solvent annealing system. The nitrogen gas is bubbled through chloroform to produce a solvent-rich vapor stream that is combined with a pure nitrogen stream prior to entering the annealing chamber. The relative flow rates of these streams were controlled by high precision mass flow controllers (Bronkhorst High-Tech B.V., F-201CV) which were rated to control flow rate to within 1% of the set

DOI: 10.1021/acsami.5b03977
ACS Appl. Mater. Interfaces 2015, 7, 16536−16547

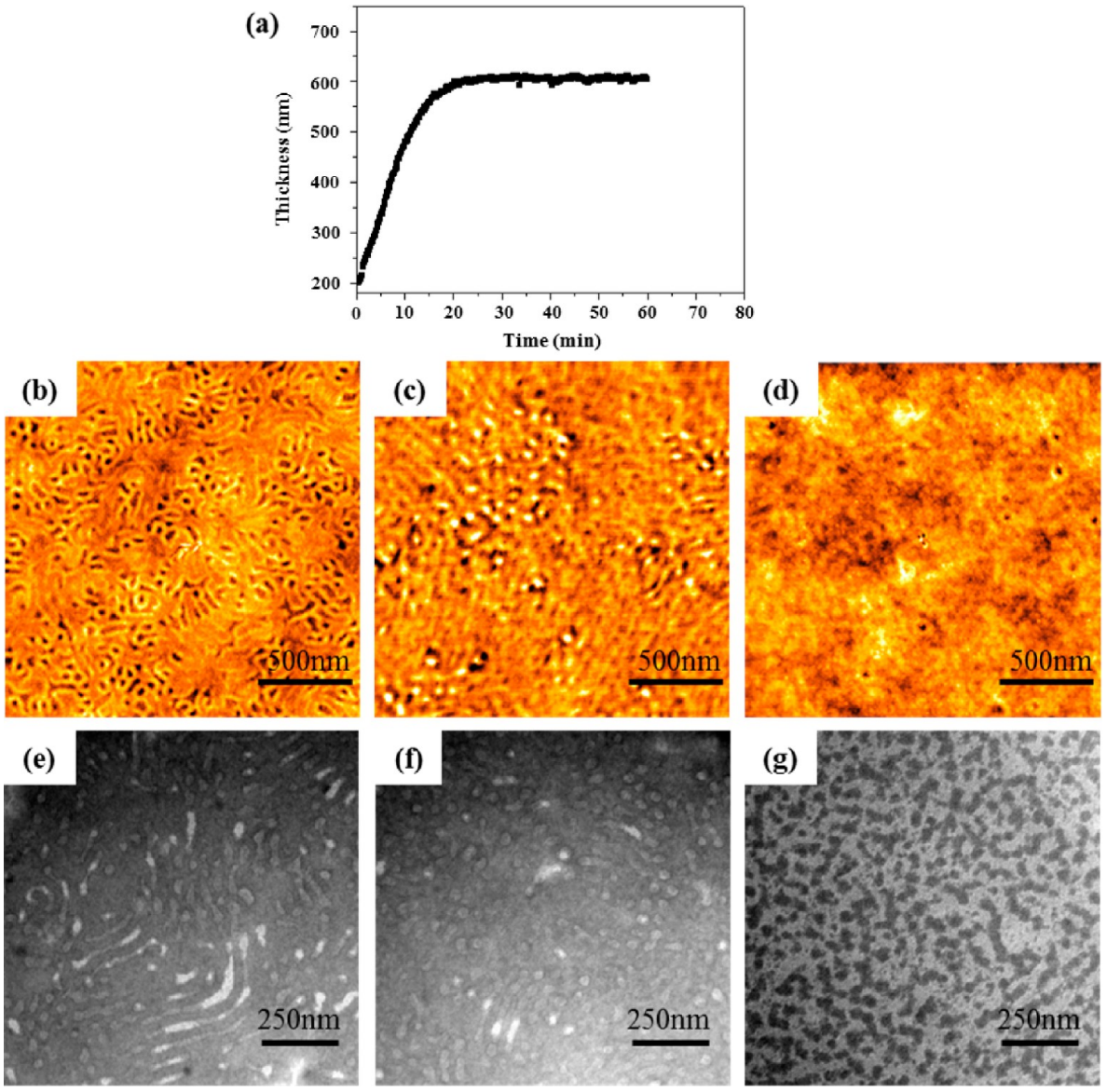

Figure 1. (a) Thickness profile of PS−PLLA thin film with initial thickness of 200 nm using chloroform as a solvent for swelling at 25 °C. (b−d) Tapping-mode AFM height images and (e−g) TEM images of the PS−PLLA thin film annealed with chloroform vapor for (b and e) 20, (c and f) 40, and (d and g) 60 min, respectively.

point and had a total range of 0−100 sccm to manipulate the vapor pressure of chloroform in the annealing chamber and thus control the swollen film thickness. The annealing chamber (~100 cm^3) was made of stainless steel and consisted of an in-and-out port with a removable sealed quartz window, which allowed for in situ measurements from a spectral reflectometer (Filmetrics, Inc., F20−UV, 250−1500 nm). The quartz window was tightly sealed by utilizing a perfluoroelastomer O-ring to minimize interaction with solvent annealing vapors. A schematic illustration and a photo of the actual solvent annealing setup are shown in Figure S1 (SI). The solvent annealing was held at ambient temperature to minimize the effect of thermal gradients that could occur in the system. Different evaporation rates were achieved in the following manner: the solvent bubble pipeline was instantaneously stopped, and the pure nitrogen pipeline was kept pumping with different flow rates to dilute the solvent vapor. The evaporation rate of the solvent vapor can be controlled by purging the pure nitrogen with different flow rate.

Simulation. The computer graphics of various cross sections cutting parallel to the particular crystallographic planes of the gyroid phase with given volume fraction was calculated. The double gyroid networks were generated by applying the parallel surface method to the minimal surface of the gyroid phase that is given by the following trigonometric approximation:[50]

$$f(x, y, z) = 2.75((\sin 2x)(\sin z)(\cos y) + (\sin 2y)(\sin x)(\cos z) + (\sin 2z)(\sin x)(\cos y)) - ((\cos 2x)(\cos 2y) + (\cos 2y)(\cos 2z) + (\cos 2z)(\cos 2x)) \quad (1)$$

Atomic Force Microscope (AFM). Tapping-mode AFM images of thin-film samples were obtained. To clearly examine the characteristic plane of the gyroid and cylinder nanostructures at the air surface, we hydrolyzed thin-film samples for 5 min, giving the required height contrast for AFM. Furthermore, to examine the bottom-view morphology, we stripped thin-film samples from the functionalized SiO_2 substrate using 1% HF solution for 30 s, floated them on the surface of water, and finally collected another clean wafer on the reverse side. A Seiko SPA-400 AFM with a SEIKO SPI-3800N Abetz probe station was utilized at room temperature. A rectangular silicon tip was used in dynamic force mode (DFM) experiments with a spring force of 5 N m^{-1} and a scan rate of 1 Hz.

DOI: 10.1021/acsami.5b03977
ACS Appl. Mater. Interfaces 2015, 7, 16536−16547

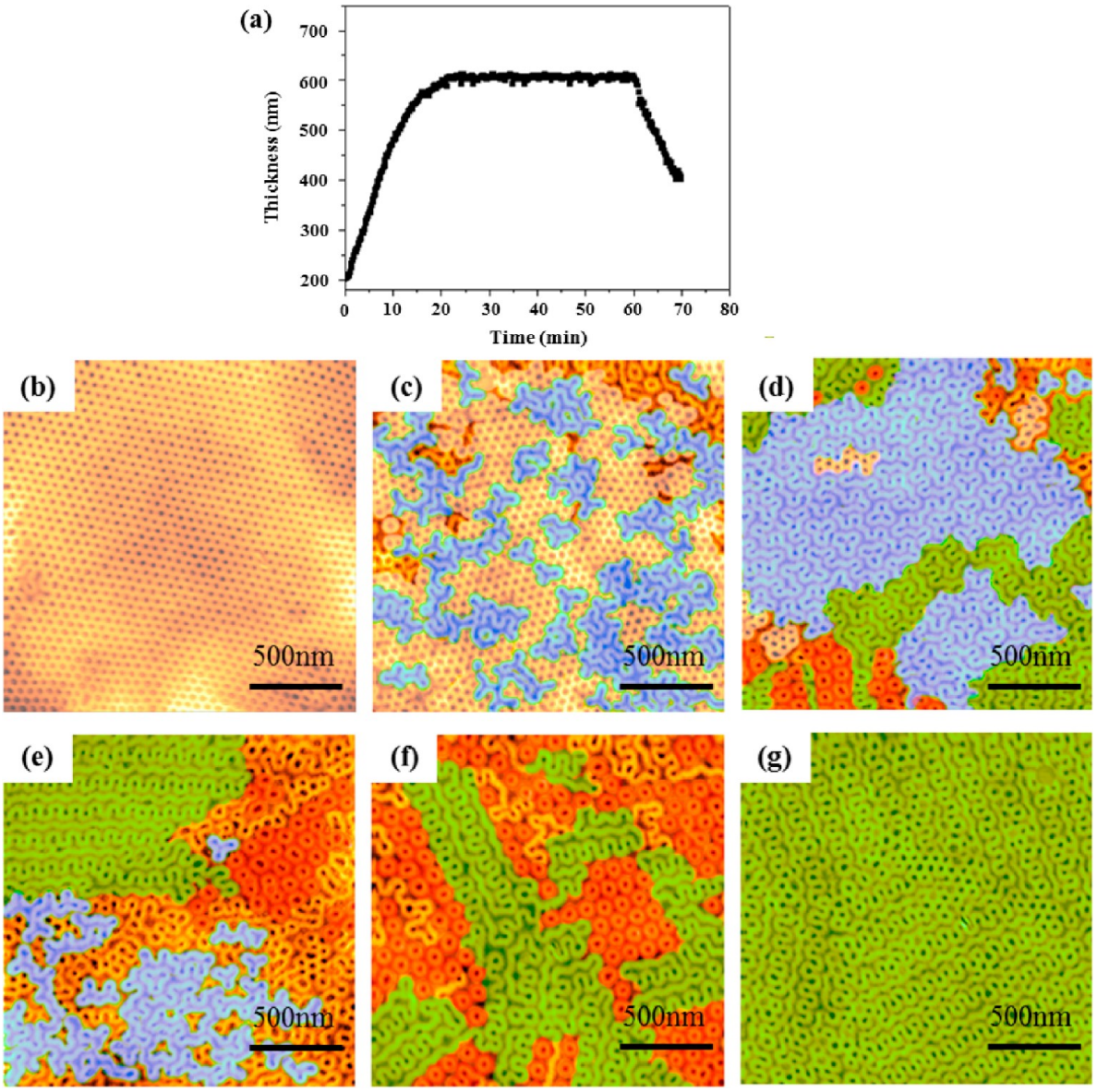

Figure 2. (a) Thickness profile of PS−PLLA thin-film during solvent annealing and controlled evaporation process. Tapping-mode AFM height images of thin-film with initial thickness of 200 nm using chloroform as solvent for swelling at 25 °C, followed by evaporation at 20 nm/min to thicknesses of (b) 550, (c) 520, (d) 490, (e) 460, (f) 430, and (g) 400 nm. The observed morphologies are marked with different colors: perpendicular cylinder (yellowish), $(111)_G$ plane of gyroid (blue), $(110)_G$ plane of gyroid (red) and $(211)_G$ plane of gyroid (green).

Transmission Electron Microscopy (TEM). To acquire the TEM images, we stripped thin-film samples from the functionalized SiO_2 substrate using 1% HF solution for 30 s, then floated them on the surface of water, and finally collected them with copper grids. To examine the cross-sectional morphology, we picked up thin-film samples stripped from the functionalized SiO_2 substrate with a piece of polyimide thin plate. A thin layer of carbon was then sputtered onto the surface of thin-film before being embedded with epoxy resin. The epoxy embedded thin-film samples were microtomed normal to the film plane at a thickness of 50 nm and then transferred onto a copper grid. All of the samples were stained with RuO_4 by exposing the samples to the vapor of 4% aqueous solution of RuO_4 for 3 h to enhance the mass−thickness contrast before the TEM observation. A JEOL JEM-2100 transmission electron microscope was used at an accelerating voltage of 200 kV.

RESULTS AND DISCUSSION

Morphological Evolution as a Function of Swollen Thickness During Evaporation. PS−PLLA thin films were prepared onto functionalized silicon wafer by spin coating using chlorobenzene solution. For the development of complete gyroid texture, the thickness of spin-coated thin film was controlled to be larger than the lattice constant of the gyroid-forming PS−PLLA (approximately 100 nm). Note that the final morphology of the PS−PLLA thin film is very sensitive to the film thickness.[32] As a result, a thin film with thickness of 200 nm was prepared to satisfy the criteria of commensuration. As shown in Figure S2 (SI), the as-cast film appears with poorly ordered structures, resulting from extremely fast evaporation rate of solvent during spin coating. To get the ordering, we treated the film with chloroform for swelling, followed by solvent evaporation. In the swollen stage, the thin-film was swollen to a different preset thickness using chloroform vapor, and the film thickness was monitored by spectral reflectometer. To carry out the solvent annealing for swelling, we prepared the chloroform vapor pressure in the chamber to reach a steady

DOI: 10.1021/acsami.5b03977
ACS Appl. Mater. Interfaces 2015, 7, 16536−16547

state after the UV signals of chloroform remain unchanged. Note that the morphology of the thin-film at the initial stage of solvent evaporation will significantly affect the evolution of morphology during solvent evaporation.[31] To alleviate the effect of initial morphologies on the following ordering process, the thin films were swollen by chloroform to reach approximately three times the initial thickness to get the disordered state at the end of swollen stage. It is also noted that uniform thickness profile in the nanostructured thin films is required for practical applications. As found, there is no dewetting problem by swelling the thin film for three times the initial thickness during the whole swelling process, as evidenced by polarized light microscopy (PLM) observation (Figure S3, SI).

Figure 1a shows the thickening profiles of 200 nm films swollen by chloroform at 25 °C. When the temperature is at the ambient condition, the vapor pressure of the chloroform ($P^*_{chloroform} \sim 158$ mmHg at 20 °C) is high enough to give high evaporation rate. Meanwhile, the cross-section area of the solvent tank is relatively larger than that of the inlet tube of the nitrogen gas. Consequently, the vapor pressure of the solvent vapor through the bubbler is referred as saturated vapor pressure. Ross et al. derived the following equation to calculate the vapor pressure of chloroform[51]

$$P_{chloroform} = P^*_{chloroform}\left(\frac{q_{chloroform}}{q_{chloroform} + q_{N_2}}\right) \quad (2)$$

where q_i, P_i, and P_i^* represent the molar flow rate (mol/min), partial pressure and saturated vapor pressure of component i, respectively. In this study, the vapor pressure of chloroform for solvent annealing was controlled to $P/P^* = 0.95$, where P is the vapor pressure of chloroform in the annealing chamber and P^* is the saturated vapor pressure at 25 °C. As shown in Figure 1a, the sample thickness increases linearly with annealing time and the film thickness will eventually reach three times the initial thickness of the film due to a level-off process for thickening at $P/P^* = 0.95$. When the thickness of the solvent swollen film is increased to three times, the swollen BCP becomes disordered due to the solvation effect that will increase the mobility of the BCP chain for reorganization. To ensure that the thin-film sample becomes disordered, we observed the developed morphologies at different swollen stages by AFM and TEM after instantaneously removal of the solvent from the film through a sudden burst of N_2 which deswells the swollen films within few seconds. Figure 1b–g shows the AFM and TEM results of PS–PLLA thin films after swelling in chloroform vapor under the swollen thickness at 600 nm for 20, 40, and 60 min, respectively. With the increase of solvent annealing time, the initial bicontinuous-like thin-film morphology will gradually transforms into disordered texture (Figure 1d,g). Subsequently, solvent evaporation (corresponding to the reduction in the film thickness) was carried out to induce the ordering of the thin film from swollen state. The ordered morphologies driven by solvent evaporation at different stages (i.e., various thicknesses) will be kinetically trapped by instantaneous removal of the solvent.

Upon solvent evaporation, the effective Flory–Huggins interaction parameters (χ_{eff}) between the PS and PLLA blocks will gradually increase due to the decrease on the solvent content. Consequently, the swollen BCP thin films in disordered state will start ordering after the initiation of solvent evaporation. By controlling the flow rate of purging N_2 gas, the solvent removal rate can be tuned to reduce the sample thickness at a constant rate. Figure 2a shows the thickness profile of the film under solvent evaporation at 20 nm/min solvent removal rate. Figure 2b shows the trapped morphologies from the swollen PS–PLLA thin-film after solvent evaporation for a solvent removal rate of 20 nm/min to give sample with 550 nm thickness; a chloroform solvent. The chloroform solvent will preferentially associate with the PS microdomain, resulting in the change of the effective volume fraction, and hence the gyroid-forming samples will transform into the cylinder morphology. Moreover, the formation of perpendicular cylinder from the solvent evaporation is attributed to kinetic factor of the swelling process.[31] As the film thickness reduces to 520 nm, an interesting phase transition from hexagonally packed perpendicular cylinders to gyroid texture with the crystallographic plane of $(111)_G$ parallel to the air surface can be found. The coexisting planes of hexagonal array of perpendicular cylinder and gyroid $(111)_G$ suggest that the initiation of phase transition in the thin-film was originally from cylinder to gyroid (Figure 2c). For the swollen thin-film with thickness of 490 and 460 nm, the gyroid characteristic crystallographic plane of $(111)_G$ will rapidly transforms into $(110)_G$ and $(211)_G$, resulting in the coexist planes of all these planes (Figure 2d,e). Further decrease in the film thickness to 430 nm, the coexisting gyroid planes of $(110)_G$ and $(211)_G$ were found without any $(111)_G$ plane (Figure 2f). As shown, hexagonally packed nanoarrays can be observed, suggesting the formation of perpendicular cylinders. The forming cylinder morphology is attributed to the partial selectivity of the in Figure 2g, the gyroid plane of $(211)_G$ plane only can be observed when the film thickness reaches to 400 nm. Accordingly, the control of morphological evolution can be achieved by solvent evaporation that enables the formation of a variety of thin-film textures with controlled orientation. The evaporation process will accompany a significant reduction in chain mobility and the morphological evolution will be suppressed when the polymer mixture reaches vitrified state.[32] As a result, the thinning process from solvent evaporation will be halted once the sample thickness reaches two times the initial thickness of the cast film.

Induced Ordering from Air Surface. As observed above, interesting phase transition behaviors were found in swollen PS–PLLA thin-film using chloroform, a PS selective solvent, during solvent evaporation. The selectivity of chloroform solvent will prefer to segregate the PS block to the air surface. Consequently, the variation of relative amount of constituted components at the air surface will result in the formation of a variety of transitional phases during the evaporation stage. Upon the solvent evaporation, the segregation strength will increase with time, and therefore, the swollen PS microdomain will preferentially experience the phase transformation from disorder to cylinder phase. Owing to the selectivity of the solvent, the formation of cylindrical morphology from disordered phase can be achieved once the concentration of the BCP is high enough to achieve ordering through the self-assembling process. The formation of perpendicular cylinders after solvent evaporation can be explained by the following mechanism. Initially, as the solvent begins to evaporate, the film is subjected to an ever-changing commensurability condition because the ratio of the film thickness (t) to the nanostructure domain spacing of the swollen film (L) (i.e., t/L) changes accordingly. To accommodate this change, the parallel orientation will incur higher energy penalties (in the form of

DOI: 10.1021/acsami.5b03977
ACS Appl. Mater. Interfaces 2015, 7, 16536–16547

chain stretching/compression or nucleation of islands/holes) compared with the perpendicular orientation.[31] As a result, to avoid energy penalties and to correspond with the commensuration for the consideration of thermodynamic stability will lead to the formation of perpendicular cylinders rather than parallel cylinders. Also, the evaporation may induce the formation of perpendicular orientation of cylinder microdomains due to the permeation discrepancy between phase-separated microdomains.[27] Further, evaporation will lead to the decrease of swelling level of PS microdomain, resulting in phase transition from cylinder to gyroid. The phase transition process will follow epitaxial relationship in which the cylinder axial direction, and the $(111)_G$ must be matched. Consequently, coexisting planes of hexagonal perpendicular cylinder and $(111)_G$ can be observed.

Nevertheless, different projection planes of the gyroid phase will possess different surface composition ratio which will result in complicate crystallographic plane transition for the gyroid nanostructure. To gain better understanding of the morphological evolution of the gyroid nanostructure during solvent annealing, we calculated the compositional fraction of the PS matrix on various crystallographic planes ($fs(X_0)$). The position of a cross-sectional plane cut parallel to a particular crystallographic plane (hkl) is defined by $h(X - X_0) + kY + lZ = 0$, X_0 is the position of the cross section, which is reduced with respect to the length of the cell edge ($0 \leq X_0 \leq 1$).[18,32] Considering of the intrinsic PS compositional fraction (~0.6) and the use of PS selective solvent, the calculated area fraction $fs(X_0)$ at different X_0 was examined and analyzed from 0.5 to 0.65.

Figure 3 plots the $fs(X_0)$ against X_0 for various crystallographic planes. It is interesting to recognize that only the planes

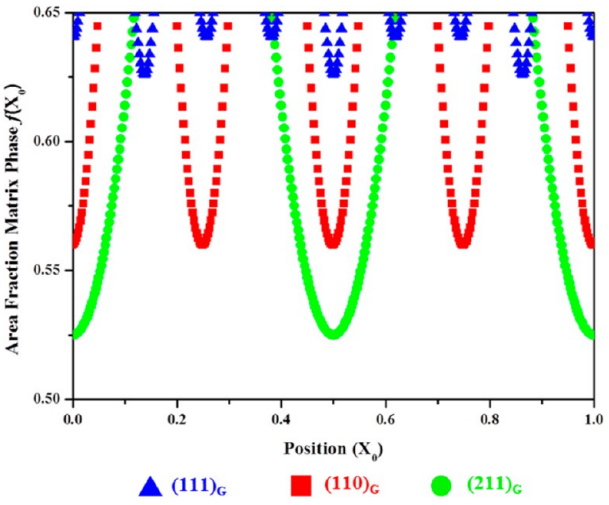

Figure 3. Plot of calculated area fraction of the matrix phase (i.e., PS), $fs(X_0)$, cutting along the planes parallel to various crystallographic planes, versus X_0. The $fs(X_0)$ are in the range of 0.5–0.65.

parallel to $(211)_G$ (green ●), $(110)_G$ planes (red ■), and $(111)_G$ planes (blue ▲) can give the PS compositional fractions ranging from 0.5 to 0.65. Also, as found, the $(211)_G$ planes at $X_0 = 0$, 0.5, and 1.0 give a minimum value of $fs(X_0)$ at 0.52, the $(110)_G$ planes at $X_0 = 0$, 0.25, 0.5, 0.75, and 1.0 give a minimum value of $fs(X_0)$ at 0.56, and the $(111)_G$ planes at $X_0 = 0.1375$, 0.5, and 0.8625 give a minimum value of $fs(X_0)$ at 0.626. Corresponding computer graphics of the 2D images parallel to the $(211)_G$, $(110)_G$, and $(111)_G$ planes at different X_0 values are shown in Figure S4 (SI). As shown in Figure 2e, characteristic $(211)_G$, $(110)_G$, and $(111)_G$ planes coexist at the free surface, indicating the phase transformation from cylinder to gyroid. However, the transitions among different crystallographic planes in gyroid are much more complicate than cylinder phase; as analyzed above, there are various compositional fractions in different projection of planes. It is noted that the phase transition is induced by the surface affinities between the solvent and the constituted blocks. The PLLA has a lower surface energy (38.3 mN/m) than PS (40.7 mN/m) at 25 °C. As shown in Figure 3, at higher PS compositional range, the gyroid morphology can be present with the crystallographic planes of $(211)_G$, $(110)_G$, and $(111)_G$. During solvent evaporation, solvent content in the swollen thin film will gradually decrease so that the selectivity effect will be deteriorated with the increase of evaporation time. Subsequently, the fraction of the lower surface energy block (PLLA) at the air surface will be increased due to the effect of surface energy on aggregation. As a result, the $(111)_G$ plane will gradually disappear, giving to the coexistence of the $(211)_G$ and $(110)_G$ planes at the air-surface (Figure 2f); namely, the surface composition of PS fraction should be reduced in the range of 0.56–0.626 (Figure 3). With further evaporation, a gyroid with exclusive characteristic $(211)_G$ plane at the surface of the thin-film can be found due to the balanced effects of surface energy and solvent selectivity (Figure 2g). Obviously, the observed transitions for the gyroid nanostructure at the air-surface is attributed to the competition of affinities of the solvent and the surface tension of the constituted blocks. Therefore, upon evaporation of the chloroform, the surface energy is able to be balanced by the selectivity of solvent to give neutral surface ($fs(X_0)$ near to 0.5).

Morphological Evolution with Various Solvent Evaporation Rates. To further examine, the effect of solvent evaporation on the behavior of phase transitions, we examined the morphological evolution by varying the evaporation rate of solvent. In contrast to the relatively high evaporation rate of 20 nm/min, slower evaporation rate was conducted by using the same solvent but lower N_2 gas purging rate, giving a lower reduction rate in thickness, as shown in Figures 4a and 5a for solvent removal rate at 10 and 5 nm/min, respectively. With decreasing the thickness of the film with reduction rate from 20 nm/min to 10 nm/min, it is difficult to acquire fully developed perpendicular cylinders but instead there are always the mixed-type morphologies with parallel and perpendicular cylinders when thickness is reduced to 550 nm as shown in Figure 4b. When thickness is reduced to 520 nm under 10 nm/min solvent removal rate (Figure 4c), the morphology of the film with the coexisting parallel and perpendicular cylinders will transform to a coexist morphology of perpendicular cylinder and gyroid $(211)_G$. This morphological evolution indicates that the parallel cylinder phase will directly transform to the $(211)_G$ prior to the perpendicular one under lower evaporation rate. This interesting morphological transition can be explained by the following mechanism. As mentioned in the previous section, film thickness is an ever-changing state during the evaporation process. Consequently, the development of parallel cylinders will compress the polymer chains to correspond with the commensurability during the solvent evaporation stage. When polymer chains are compressed, the average nearest-neighbor distance between the chemical junctions will inrease and lead to the change of interfacial curvature. The change in the interfacial curvature will result in the phase transition from

DOI: 10.1021/acsami.5b03977
ACS Appl. Mater. Interfaces 2015, 7, 16536–16547

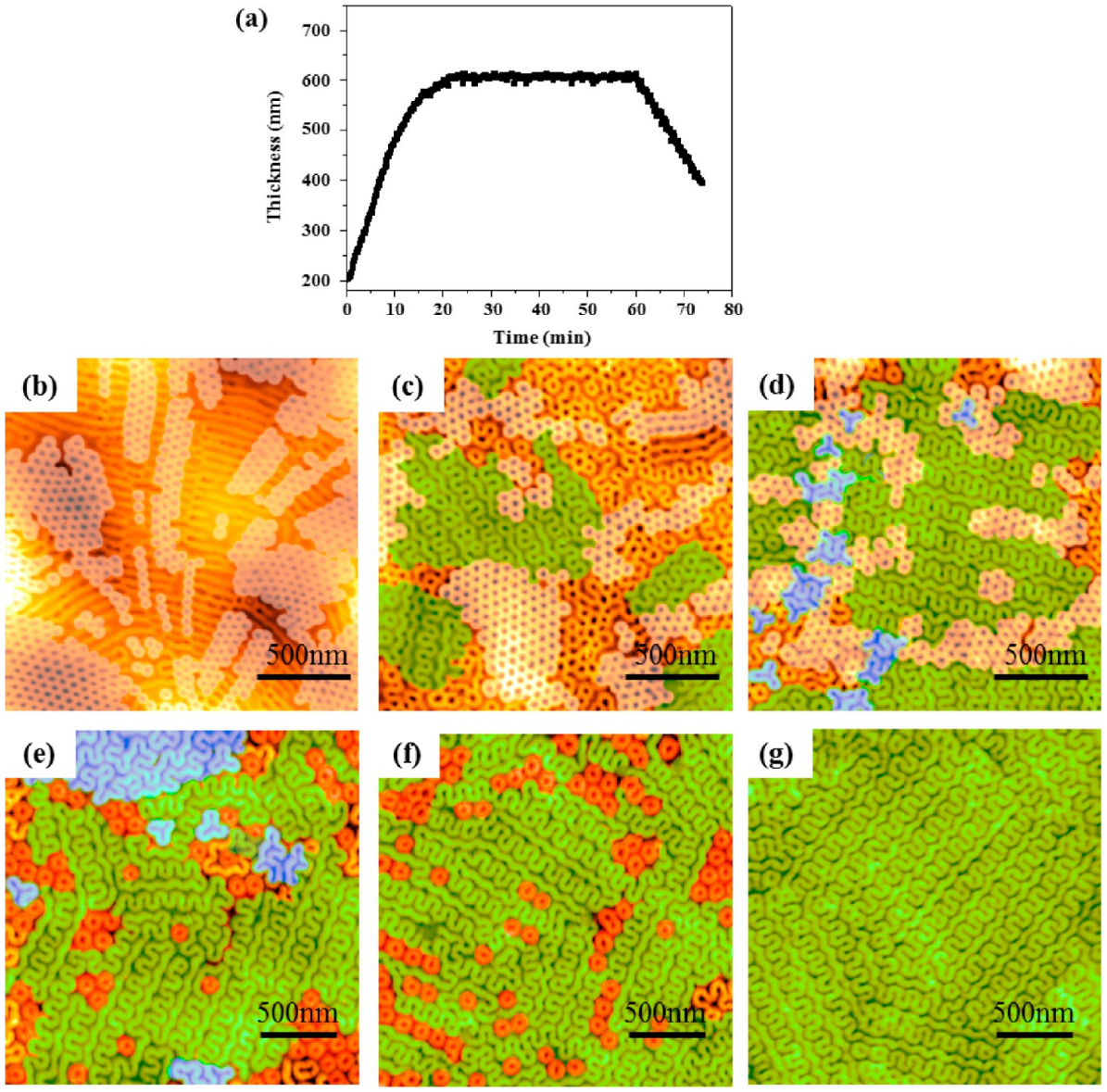

Figure 4. (a) Thickness profile of PS−PLLA thin-film in solvent annealing and evaporation process. Tapping-mode AFM height images of the PS−PLLA thin film with initial thickness of 200 nm using chloroform as solvent for swelling, followed by evaporation at 15 nm/min to thicknesses of (b) 550, (c) 520, (d) 490, (e) 460, (f) 430, and (g) 400 nm. The observed morphologies are marked with different colors: (yellowish) perpendicular cylinder, (blue) $(111)_G$ plane of gyroid, (red) $(110)_G$ plane of gyroid, and (green) $(211)_G$ plane of gyroid.

the parallel cylinder to the gyroid morphology. In contrast, during the solvent evaporation process, perpendicular cylinder morphology could easily adjust the distance between polymer chains along the direction of the cylinderical axis without fluctuation of effective volume fraction. Therefore, we speculate that the parallel cylinders should directly transform to gyroid morphology prior to perpendicular cylinders. The formation of the perpendicular cylinders is a kinetic cause from fast evaporation, whereas the phase transition from parallel cylinder to gyroid is attributed to thermodynamic origins so that the transformation will take over directly without the formation of perpendicular cylinders under slow evaporation. Also, during the transformation from parallel cylinder to gyroid, the thickness is reduced to 520 nm under 10 nm/min solvent removal rate, (10) plane of cylinders (parallel cylinder) should transform to $(211)_G$.[15] As a result, the coexisting planes of perpendicular cylinder and $(211)_G$ was observed (Figures 4c). With further decrease in the film thickness to 490 nm, the perpendicular cylinders will also start to transform into gyroid. As shown in Figure 4d, the coexisting planes of perpendicular cylinders and gyroids $(111)_G$ and $(211)_G$ can be clearly observed. This observation further confirms that the parallel cylinders will first transforms into gyroid morphology prior to become perpendicular cylinders. The gyroid coexisting planes of $(111)_G$, $(110)_G$, and $(211)_G$ (Figure 4e) will gradually transform into the coexisting planes of $(110)_G$ and $(211)_G$ (Figure 4f) and finally the becomes exclusive $(211)_G$ gyroid plane when the film thickness reaches to 400 nm (Figure 4g).

When the solvent removal rate is further decreased to 5 nm/min, there is no formation of perpendicular cylinders from the parallel cylinders, which is due to the annihilation of perpendicular cylinder formation under slow evaporation (Figure 5b). With a further decrease in the solvent removal rate, the effect of energy penalties for the parallel orientation

DOI: 10.1021/acsami.5b03977
ACS Appl. Mater. Interfaces 2015, 7, 16536−16547

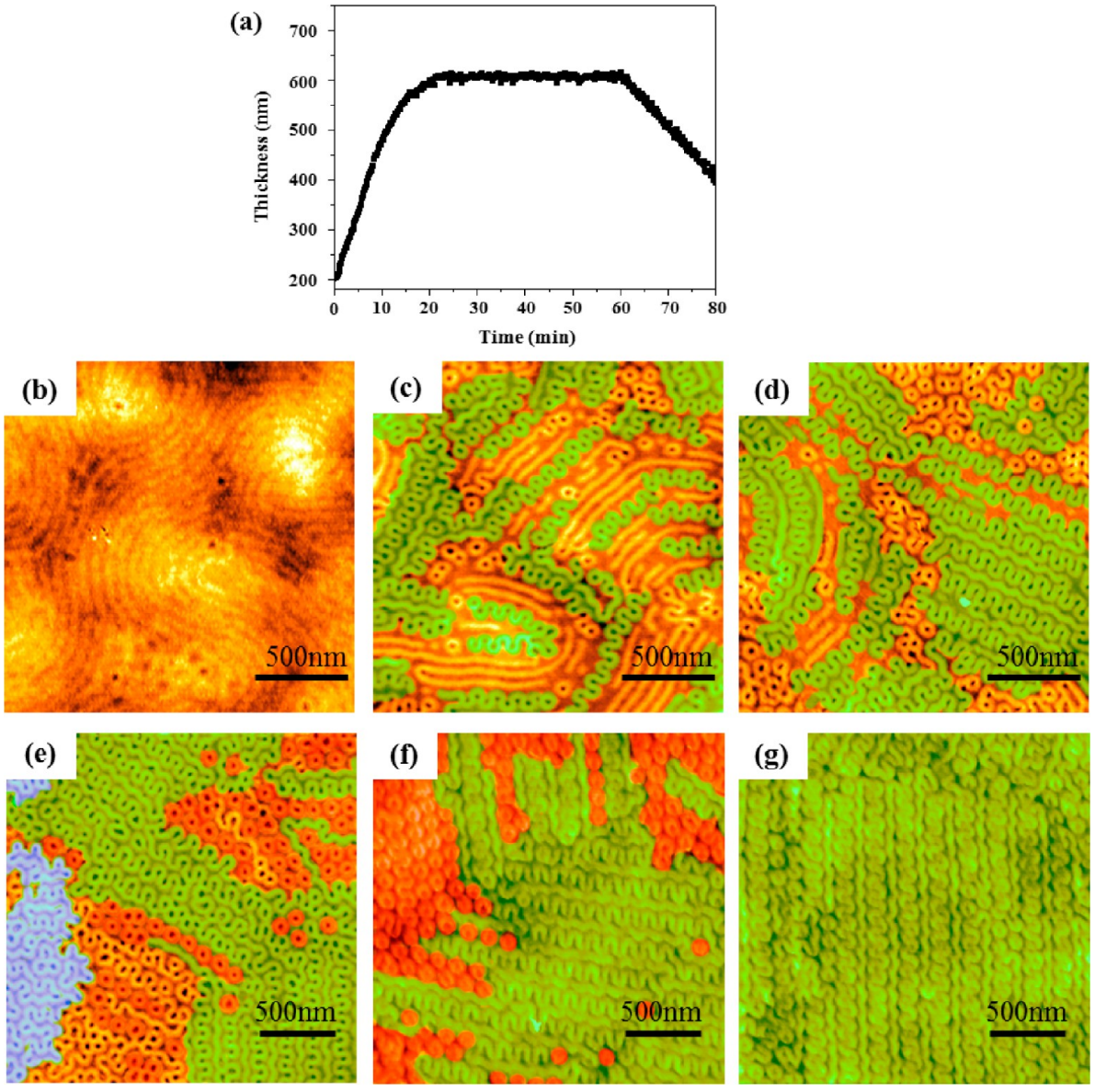

Figure 5. (a) Thickness profile of PS−PLLA thin-film in solvent annealing and evaporation process. Tapping-mode AFM height images of the PS−PLLA thin film with initial thickness of 200 nm using chloroform as solvent for swelling, followed by evaporation at 10 nm/min to thicknesses of (b) 550, (c) 520, (d) 490, (e) 460, (f) 430, and (g) 400 nm. The observed morphologies are marked with different colors: (yellowish) perpendicular cylinder, (blue) $(111)_G$ plane of gyroid, (red) $(110)_G$ plane of gyroid, and (green) $(211)_G$ plane of gyroid.

(in the form of chain stretching or compression) will mitigate, and the influence of the enthalpy contribution from the interfacial interaction will be enhanced. Consequently, for the lower evaporation rate condition, the thermodynamic stability will lead the formation of parallel cylinders rather than perpendicular cylinders as expected (Figure 5a). When thickness is reduced to 520 and 490 nm, a coexisting planes of parallel cylinders and gyroid $(211)_G$ can be observed (Figure 5b,c). Finally, the morphological evolution of gyroid upon solvent evaporation will follow the same route mentioned above, as shown in Figure 5e−g.

To analyze the observed morphologies, we constructed a transient PS−PLLA morphology diagram (Figure 6) in which various morphologies are plotted as solvent removal rate versus swollen thickness based on the results of the observed AFM images from Figures 2, 4, and 5. The phase diagram can be divided into three regions and each region corresponds to

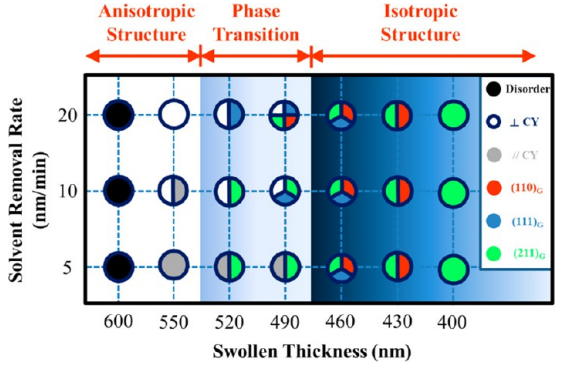

Figure 6. Phase behavior of PS−PLLA thin-film upon solvent evaporation as a function of solvent removal rate and swollen thickness. The corresponding morphology for each symbol are listed at the right corner (CY → cylinder, $(xxx)_G$ → xxx plane of gyroid).

DOI: 10.1021/acsami.5b03977
ACS Appl. Mater. Interfaces 2015, 7, 16536−16547

different stage of morphological evolution from solvent evaporation. The first region (i.e., the ordering process from disorder to cylinder) is denoted as anisotropic structure region. In this region, the orientation of the cylinder is highly related to the solvent evaporation rate due to kinetic origin as shown in the phase diagram at which the fast evaporation will lead to the formation of perpendicular cylinder, whereas the slow one gives parallel cylinder formation. The second region is the coexisting morphologies of cylinder and gyroid which is denoted as phase transition region. The observed coexisting morphologies are highly dependent on the orientation of the cylinder structure in the first region. A different orientation of cylinder as formed in the first region will give rise to different crystallographic plane of the gyroid phase upon solvent evaporation. The third region is denoted as isotropic structure region. The vocabulary "isotropic" and "anisotropic" have usually been used in optics. Light gets polarized when transmitted through a structured liquid containing such optical anisotropy. Therefore, noncubic structures (lamellar or cylinder) are birefringent objects, and transmitted light intensity will get recorded at the detector of the polarized light microscope. By contrast, cubic ordered morphologies do not have any unique crystallographic optical axis and hence do not show birefringence. Disordered states in block copolymers have concentration fluctuations that are random in nature with no preferred spatial orientation and thus are nonbirefringent. For both cubic states and disordered states, the detector will give zero transmitted light intensity. As a result, the absence of the birefringence for the gyroid structure (cubic structure) was examined and regarded as a isotropic structure.[52] The gyroid morphologies are transformed into different crystallographic planes due to thermodynamics origin. Accordingly, the transitions of the gyroid morphologies within this region are independent of solvent evaporation rate. We speculate that the discrepancies between phase transition mechanisms of the first and third regions are attributed to the differences between anisotropy and isotropy of the structures. The orientation of the anisotropic cylinder structure will be affected by the flow field attributed to the evaporation of the solvent. In contrast, the orientation of the isotropic gyroid is mainly attributed to the affinity and surface tension factor. In conclusion, the morphological evolution of PS−PLLA thin-film should be strongly dependent upon the solvent removal rate only in the initial stage of the deswollen process which is attributed to the anisotropy of cylinder structure. Once the morphology is transformed to the isotropic gyroid structure after longer deswelling time, the morphological evolution will be largely controlled by the variation of the surface composition resulting from the thermodynamic effect.

Induced Ordering from Functionalized Substrate. As mentioned above, the partially PS selective solvent, chloroform, can be used for solvent annealing followed by solvent evaporation to acquire the transitional phase from cylinder to gyroid. Consequently, PS−PLLA thin film with ordered and oriented crystallography plane of gyroid (i.e., $(211)_G$) can be found at the air surface. However, in practical applications, especially for the fabrication of high porosity structure, thin films with open-cell and span-through character are needed to carry out the hydrolysis of PLLA. The cross-sectional TEM images were obtained for further examination of different morphological transitions in the thin-film. Figure 7a shows the results of the PS−PLLA thin-film sample treated by solvent annealing (1 h at 600 nm swollen thickness) followed by evaporation rate of 20 nm/min to 400 nm. The cross-sectional

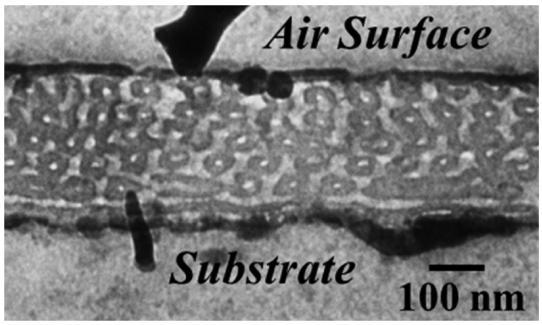

Figure 7. Cross-sectional TEM image of PS−PLLA thin-film with the initial PS−PLLA thickness of 200 nm treated by solvent annealing followed by evaporation of solvent removal rate at 20 nm/min to 400 nm on different functionalized SiO_2 substrates.

TEM image shows the $(110)_G$ projection of the gyroid phase extending from the film surface to the substrate, suggesting the feasibility to acquire the gyroid morphology with controlled orientation by controlled evaporation process of solvent swollen thin-film. However, a bright straight line near the substrate can still be clearly identified (Figure 7), indicating the formation of a single-layer cylinder near the substrate. The parallel oriented cylinder near the substrate is attributed to the strong enthalpic interaction of the substrate which is fully grafted with PS−OH homopolymers. The phase morphology near the substrate can be further confirmed from the bottom-view AFM images. As shown in Figure 8a, no clear image contrast can be identified, even after hydrolytic treatment, indicating that the PS block should be wetted onto the substrate.

To eliminate the PS wetting layer, the PLLA−OH was further functionalized onto the SiO_2 substrate to balance the surface preferentiality of the substrate. A relatively neutral substrate (SUB-0) was prepared by using a two-step grafting processes through thermal annealing at which PS−OH can be grafted onto SiO_2 surface at 100 °C for 120 min followed by grafting of PLLA−OH.[44]

The thin-film sample with the initial thickness of 200 nm on a neutral substrate was treated under the same processing condition (1 h solvent annealing at 600 nm swollen thickness followed by evaporation of solvent removal rate at 20 nm/min to 400 nm). Similarly, the thin-film morphology consisting of $(211)_G$ at the air surface can be found. However, even with the modification of the substrate with neutral selectivity, no significant image contrast can be identified from the bottom-view AFM image after hydrolytic treatment (Figure 8b). This result shows the similar phenomenon as described in our previous work,[32] the PS chains on the functionalized substrate will be stretched by chloroform (PS selective solvent) during the solvent evaporation process while the PLLA chains will recoil. Consequently, surface preferentiality of the functionalized SiO_2 surface is further tuned by increasing the proportion of PLLA−OH on functionalized substrate. As demonstrated in our previous report, the proportion of PLLA was precisely calculated from the XPS spectra. The calculated proportion of PLLA gradually increases while the thermal annealing time for the grafting of the PS−OH brushes decreases. Consequently, the results indicate that the composition ratio of PS−OH to PLLA−OH on the SiO_2 surface can be effectively controlled by this two-step annealing process.[44] Accordingly, a series of functionalized substrates with steadily increased PLLA−OH

DOI: 10.1021/acsami.5b03977
ACS Appl. Mater. Interfaces 2015, 7, 16536−16547

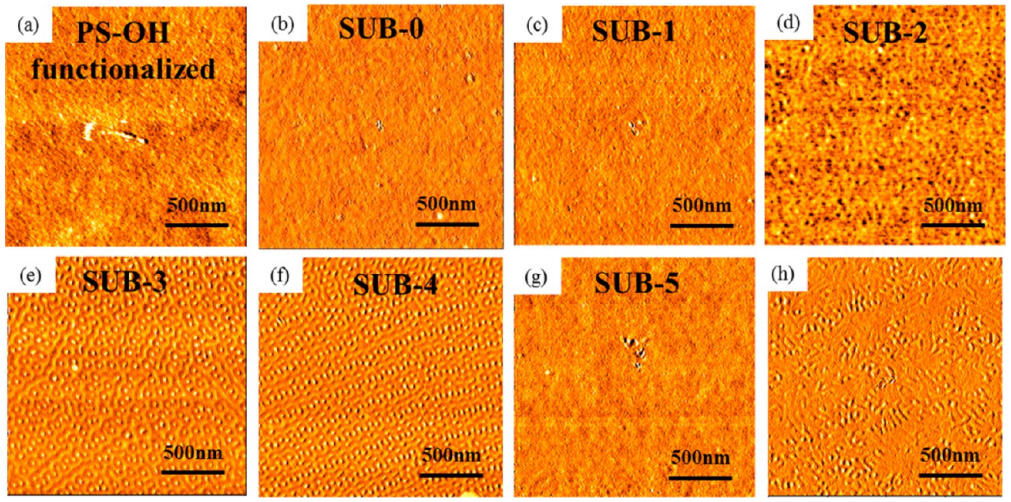

Figure 8. Tapping-mode bottom-view AFM phase images of (a) PS−OH fully functionalized substrate, (b) SUB-0, (c) SUB-1, (d) SUB-2, (e) SUB-3, (f) SUB-4, and (g) SUB-5 with the initial PS−PLLA thickness of 200 nm on functionalized SiO_2 substrates treated by solvent annealing followed by solvent removal rate of 20 nm/min. (h) Tapping-mode bottom-view AFM phase images of Figure 8g after hydrolytic treatment.

compositional fraction were prepared. The substrates were labeled as SUB-1, SUB-2, SUB-3 SUB-4, and SUB-5 for 110, 100, 90, 80, and 70 min thermal annealing to graft the PS−OH brush, respectively. As shown in Figure 8c,d (SUB-1 and SUB-2), no significant image contrast can be identified, even after hydrolytic treatment, suggesting that a thin layer of PS is wetted onto the substrate. With increasing the proportion of the PLLA brush for the functionalized substrate (SUB-3, Figure 8e) a clear microphase-separated morphology can be observed, suggesting that the composition of the grafted polymer brush starts to compensate the effect of solvent selectivity. Similar results can also be found in SUB-4 (Figure 8f). Furthermore, the bottom-view morphologies between SUB-3 and SUB-4 show an interesting discrepancy; the bottom-view image of the SUB-3 sample shows the coexisting planes of $(110)_G$ and $(211)_G$, whereas the preferential plane of $(211)_G$ can only be found in the plane of SUB-4 sample. This morphological variation is indeed in line with the morphological results as described above. By increasing the proportion of the grafted PLLA brush, it is possible to reduce the preferentiality of the substrate for the PS block and to enhance the preferentiality of the substrate for the PLLA block simultaneously. Consequently, preferential $(110)_G$ and $(211)_G$ planes will gradually transforms into $(211)_G$ plane due to the consideration of equivalent composition. Further increasing the proportion of the PLLA brush (SUB-5, Figure 8g), no significant image contrast can be identified. In contrast to SUB-1, a clear microphase-separated image can be observed after hydrolytic treatment (Figure 8h), indicating that a thin-layer of PLLA should be wetted onto the substrate due to the dominant effect of substrate selectivity for the PLLA block. Although the results show similar trend as described in our previous work,[32] the neutrality of the substrate was achieved at higher PLLA fraction for the solvent evaporation process (SUB-4) than the solvent annealing process (SUB-3). We speculate that the discrepancy of the PLLA fraction for the neutral condition is attributed to the difference of the absorbed solvent amount in the swollen state. The amount of solvent contained in the thin-film is removed to induce morphologies by solvent evaporation process ($\phi_{solvent} \sim 0.67$) is higher than that by solvent annealing process ($\phi_{solvent} \sim 0.5$). The larger amount of chloroform solvent contained in the thin film will give rise to a higher selectivity toward the PS block. To compensate the higher selectivity caused by the solvent absorption, we must graft the higher proportion of the PLLA brush onto the substrate to achieve the neutral condition for during the solvent evaporation process. As a result, it is possible to balance the substrate selectivity on constituted blocks of PS−PLLA upon solvent evaporation process by tuning the characteristics of the functionalized substrates.

CONCLUSIONS

The morphological evolution of gyroid-forming block copolymer thin films was carefully studied with varying solvent evaporation rate. During the solvent evaporation process, interesting morphological evolution from disorder to cylinder (anisotropic structure), and then gyroid (isotropic structure) can be observed. Most importantly, the morphological evolution of PS−PLLA thin films is strongly dependent upon the solvent removal rate only in the initial stage of the evaporation process due to the anisotropy of cylinder structure. Once the morphology is transformed back to the isotropic gyroid structure after longer evaporation, the morphological evolution will only relate to the variation of the surface composition resulting from thermodynamic origin. Meanwhile, similar phase transitions at the substrate can also be obtained by controlling the ratio of PLLA−OH to PS−OH homopolymers functionalized the substrate. Ultimately, nanostructured gyroid thin film with the $(211)_G$ plane parallel to both interfaces was obtained. These results offer a new insight into the self-assembly of gyroid-forming PS−PLLA BCPs in the thin-film state. Furthermore, well-ordered nanoporous polymers can be fabricated after the removal of the PLLA block in the self-assembled PS−PLLA gyroid thin film and used as polymeric templates for the synthesis of a variety of nanohybrids and nanoporous inorganic materials, giving appealing applications in nanotechnology[49] such as antireflective structure (ARS) materials,[10] surface plasmon resonance (SPR) materials,[47] catalysis,[45,46] and even environment-selective delivery materials.[48]

DOI: 10.1021/acsami.5b03977
ACS Appl. Mater. Interfaces 2015, 7, 16536−16547

■ ASSOCIATED CONTENT

Supporting Information

Schematic illustration and photo of the actual solvent annealing setup, AFM images, PLM images and computer graphics of the 2D images of gyroid. The Supporting Information is available free of charge on the ACS Publications website at DOI: 10.1021/acsami.5b03977.

■ AUTHOR INFORMATION

Corresponding Author

*Tel: 886-3-5738349. Fax: 886-3-5715408. E-mail: rmho@mx.nthu.edu.tw.

Notes

The authors declare no competing financial interest.

■ ACKNOWLEDGMENTS

Financial support from the Ministry of Science and Technology, Taiwan, R.O.C., under Grant No. MOST 103-2633-M-007-001 is acknowledged.

■ REFERENCES

(1) Urade, V. N.; Wei, T. C.; Tate, M. P.; Kowalski, J. D.; Hillhouse, H. W. Nanofabrication of Double-Gyroid Thin Films. *Chem. Mater.* **2007**, *19*, 768−777.

(2) Ruiz, R.; Kang, H.; Detcheverry, F. A.; Dobisz, E.; Kercher, D. S.; Albrecht, T. R.; De Pablo, J. J.; Nealey, P. F. Density Multiplication and Improved Lithography by Directed Block Copolymer Assembly. *Science* **2008**, *321*, 936−939.

(3) Park, S.; Wang, J.-Y.; Kim, B.; Xu, J.; Russell, T. P. A Simple Route to Highly Oriented and Ordered Nanoporous Block Copolymer Templates. *ACS Nano* **2008**, *2*, 766−772.

(4) Thurn-Albrecht, T.; Steiner, R.; DeRouchey, J.; Stafford, C. M.; Huang, E.; Bal, M.; Tuominen, M.; Hawker, C. J.; Russell, T. P. Nanoscopic Templates from Oriented Block Copolymer Films. *Adv. Mater.* **2000**, *12*, 787−791.

(5) Olson, D. A.; Chen, L.; Hillmyer, M. A. Templating Nanoporous Polymers with Ordered Block Copolymers. *Chem. Mater.* **2008**, *20*, 869−890.

(6) Yang, S. Y.; Ryu, I.; Kim, H. Y.; Kim, J. K.; Jang, S. K.; Russell, T. P. Nanoporous Membranes with Ultrahigh Selectivity and Flux for the Filtration of Viruses. *Adv. Mater.* **2006**, *18*, 709−712.

(7) Phillip, W. A.; O'Neill, B.; Rodwogin, M.; Hillmyer, M. A.; Cussler, E. L. Self-Assembled Block Copolymer Thin Films as Water Filtration Membranes. *ACS Appl. Mater. Interfaces* **2010**, *2*, 847−853.

(8) Querelle, S. E.; Jackson, E. A.; Cussler, E. L.; Hillmyer, M. A. Ultrafiltration Membranes with a Thin Poly(styrene)-b-poly(isoprene) Selective Layer. *ACS Appl. Mater. Interfaces* **2013**, *5*, 5044−5050.

(9) Joo, W.; Park, M. S.; Kim, J. K. Block Copolymer Film with Sponge-Like Nanoporous Strucutre for Antireflection Coating. *Langmuir* **2006**, *22*, 7960−7963.

(10) Hsueh, H. Y.; Chen, H. Y.; She, M. S.; Chen, C. K.; Ho, R. M.; Gwo, S.; Hasegawa, H.; Thomas, E. L. Inorganic Gyroid with Exceptionally Low Refractive Index from Block Copolymer Templating. *Nano Lett.* **2010**, *10*, 4994−5000.

(11) Hobbs, R. G.; Farrell, R. A.; Bolger, C. T.; Kelly, R. A.; Morris, M. A.; Petkov, N.; Holmes, J. D. Selective Sidewall Wetting of Polymer Blocks in Hydrogen Silsesquioxane Directed Self-Assembly of PS-b-PDMS. *ACS Appl. Mater. Interfaces* **2012**, *4*, 4637−4642.

(12) Segalman, R. A.; McCulloch, B.; Kirmayer, S.; Urban, J. J. Block Copolymers for Organic Optoelectronics. *Macromolecules* **2009**, *42*, 9205−9216.

(13) Bates, F. S. Polymer-Polymer Phase-Behavior. *Science* **1991**, *251*, 898−905.

(14) Knoll, A.; Horvat, A.; Lyakhova, K. S.; Krausch, G.; Sevink, G. J. A.; Zvelindovsky, A. V.; Magerle, R. Phase Behavior in Thin Films of Cylinder-Forming Block Copolymers. *Phys. Rev. Lett.* **2002**, *89*, 035501.

(15) Hajduk, D. A.; Harper, P. E.; Gruner, S. M.; Honeker, C. C.; Kim, G.; Thomas, E. L.; Fetters, L. J. The Gyroid: A New Equilibrium Morphology in Weakly Segregated Diblock Copolymers. *Macromolecules* **1994**, *27*, 4063−4075.

(16) Schulz, M. F.; Bates, F. S.; Almdal, K.; Mortensen, K. Epitaxial Relationship for Hexagonal-to-Cubic Phase Transition in a Book Copolymer Mixture. *Phys. Rev. Lett.* **1994**, *73*, 86−89.

(17) Matsen, M. W.; Schick, M. Stable and unstable phases of a diblock copolymer melt. *Phys. Rev. Lett.* **1994**, *72*, 2660−2663.

(18) Hashimoto, T.; Nishikawa, Y.; Tsutsumi, K. Identification of the "Voided Double-Gyroid-Channel": A New Morphology in Block Copolymers. *Macromolecules* **2007**, *40*, 1066−1072.

(19) Kim, G.; Libera, M. Morphological Development in Solvent-Cast Polystyrene-Polybutadiene-Polystyrene (SBS) Triblock Copolymer Thin Films. *Macromolecules* **1998**, *31*, 2569−2577.

(20) Li, M. Q.; Ober, C. K. Block Copolymer Patterns and Templates. *Mater. Today* **2006**, *9*, 30−39.

(21) Bang, J.; Jeong, U.; Ryu, D. Y.; Russell, T. P.; Hawker, C. J. Block Copolymer Nanolithography: Translation of Molecular Level Control to Nanoscale Patterns. *Adv. Mater.* **2009**, *21*, 4769−4792.

(22) Albert, J. N. L.; Epps, T. H. Self-Assembly of Block Copolymer Thin Films. *Mater. Today* **2010**, *13*, 24−33.

(23) She, M. S.; Lo, T. Y.; Hsueh, H. Y.; Ho, R. M. Nanostructured Thin Films of Degradable Block Copolymers and Their Applications. *NPG Asia Mater.* **2013**, *5*, e42.

(24) Sinturel, C.; Vayer, M.; Morris, M.; Hillmyer, M. A. Solvent Vapor Annealing of Block Polymer Thin Films. *Macromolecules* **2013**, *46*, 5399−5415.

(25) Luo, M.; Epps, T. H. Directed Block Copolymer Thin Film Self-Assembly: Emerging Trends in Nanopattern Fabrication. *Macromolecules* **2013**, *46*, 7567−7579.

(26) Borah, D.; Shaw, M. T.; Holmes, J. D.; Morris, M. A. Sub-10 nm Feature Size PS-b-PDMS Block Copolymer Structures Fabricated by a Microwave-Assisted Solvothermal Process. *ACS Appl. Mater. Interfaces* **2013**, *5*, 2004−2012.

(27) Ho, R. M.; Tseng, W. H.; Fan, H. W.; Chiang, Y. W.; Lin, C. C.; Ko, B. T.; Huang, B. H. Solvent-Induced Microdomain Orientation in Polystyrene-b-Poly(L-lactide) Diblock Copolymer Thin Films for Nanopatterning. *Polymer* **2005**, *46*, 9362−9377.

(28) Kim, S. H.; Misner, M. J.; Xu, T.; Kimura, M. S. H.; Russell, T. P. Highly Oriented and Ordered Arrays from Block Copolymers via Solvent Evaporation. *Adv. Mater.* **2004**, *16*, 226−231.

(29) Park, S.; Wang, J. Y.; Kim, B.; Xu, J.; Russell, T. P. A Simple Route to Highly Oriented and Ordered Nanoporous Block Copolymer Templates. *ACS Nano* **2008**, *2*, 766−772.

(30) Baruth, A.; Seo, M.; Lin, C. H.; Walster, K.; Shankar, A.; Hillmyer, M. A.; Leighton, C. Optimization of Long-Range Order in Solvent Vapor Annealed Poly(styrene)-block-poly(lactide) Thin Films for Nano lithography. *ACS Appl. Mater. Interfaces* **2014**, *6*, 13770−13781.

(31) Albert, J. N. L.; Young, W. S.; Lewis, R. L., III; Bogart, T. D.; Smith, J. R.; Epps, T. H., III Systematic Study on the Effect of Solvent Removal Rate on the Morphology of Solvent Vapor Annealed ABA Triblock Copolymer Thin Films. *ACS Nano* **2012**, *6*, 459−466.

(32) She, M. S.; Lo, T. Y.; Ho, R. M. Controlled Ordering of Block Copolymer Gyroid Thin Films by Solvent Annealing. *Macromolecules* **2014**, *47*, 175−182.

(33) Peters, R. D.; Yang, X. M.; Kim, T. K.; Nealey, P. F. Wetting Behavior of Block Copolymers on Self Assembled Films of Alkylchlorosiloxanes: Effect of Grafting Density. *Langmuir* **2000**, *16*, 9620−9626.

(34) Peters, R. D.; Yang, X. M.; Kim, T. K.; Sohn, B. H.; Nealey, P. F. Using Self-Assembled Monolayers Exposed to X-rays to Control the Wetting Behavior of Thin Films of Diblock Copolymers. *Langmuir* **2000**, *16*, 4625−4631.

(35) Han, E.; In, I.; Park, S. M.; La, Y. H.; Wang, Y.; Nealey, P. F.; Gopalan, P. Photopatternable Imaging Layers for Controlling Block

DOI: 10.1021/acsami.5b03977
ACS Appl. Mater. Interfaces 2015, 7, 16536−16547

Copolymer Microdomain Orientation. *Adv. Mater.* **2007**, *19*, 4448−4452.
(36) Han, E.; Stuen, K. O.; Leolukman, M.; Liu, C. C.; Nealey, P. F.; Gopalan, P. Perpendicular Orientation of Domains in Cylinder-Forming Block Copolymer Thick Films by Controlled Interfacial Interactions. *Macromolecules* **2009**, *42*, 4896−4901.
(37) Suh, H. S.; Kang, H.; Liu, C. C.; Nealey, P. F.; Char, K. Orientation of Block Copolymer Resists on Interlayer Dielectrics with Tunable Surface Energy. *Macromolecules* **2010**, *43*, 461−466.
(38) Mansky, P.; Liu, Y.; Huang, E.; Russell, T. P.; Hawker, C. J. Controlling Polymer-Surface Interactions with Random Copolymer Brushes. *Science* **1997**, *275*, 1458−1460.
(39) Huang, E.; Rockford, L.; Russell, T. P.; Hawker, C. J. Nanodomain Control in Copolymer Thin Films. *Nature* **1998**, *395*, 757−758.
(40) Huang, E.; Russell, T. P.; Harrison, C.; Chaikin, P. M.; Register, R. A.; Hawker, C. J.; Mays, J. Using Surface Active Random Copolymers to Control the Domain Orientation in Diblock Copolymer Thin Films. *Macromolecules* **1998**, *31*, 7641−7650.
(41) Ryu, D. Y.; Shin, K.; Drockenmuller, E.; Hawker, C. J.; Russell, T. P. A Generalized Approach to the Modification of Solid Surfaces. *Science* **2005**, *308*, 236−239.
(42) Shengxiang, J.; Guoliang, L.; Zheng, F.; Craig, G. S. W.; Himpsel, F. J.; Nealey, P. F. Preparation of Neutral Wetting Brushes for Block Copolymer Films from Homopolymer Blends. *Adv. Mater.* **2008**, *20*, 3054−3060.
(43) Gu, W.; Hong, S. W.; Russell, T. P. Orienting Block Copolymer Microdomains with Block Copolymer Brushes. *ACS Nano* **2012**, *6*, 10250−10257.
(44) She, M. S.; Lo, T. Y.; Ho, R. M. Long-Range Ordering of Block Copolymer Cylinders Driven by Combining Thermal Annealing and Substrate Functionalization. *ACS Nano* **2013**, *7*, 2000−2011.
(45) Hsueh, H. Y.; Huang, Y. C.; Ho, R. M.; Lai, C. H.; Makida, T.; Hasegawa, H. Nanoporous Gyroid Nickel from Block Copolymer Templates via Electroless Plating. *Adv. Mater.* **2011**, *23*, 3041−3046.
(46) Hsueh, H. Y.; Ho, R. M. Bicontinuous Ceramics with High Surface Area from Block Copolymer Templates. *Langmuir* **2012**, *28*, 8518−8529.
(47) Hsueh, H. Y.; Chen, H. Y.; Hung, Y. C.; Ling, Y. C.; Gwo, S.; Ho, R. M. Well-Defined Multibranched Gold with Surface Plasmon Resonance in Near-Infrared Region from Seeding Growth Approach Using Gyroid Block Copolymer Template. *Adv. Mater.* **2013**, *25*, 1780−1786.
(48) Lee, H. C.; Hsueh, H. Y.; Jeng, U. S.; Ho, R. M. Functionalized Nanoporous Gyroid SiO_2 with Double-Stimuli Responsive Properties as Environment-Selective Delivery Systems. *Macromolecules* **2014**, *47*, 3041−3051.
(49) Hsueh, H. Y.; Yao, C. T.; Ho, R. M. Well-Ordered Nanohybrids and Nanoporous Materials from Gyroid Block Copolymer Templates. *Chem. Soc. Rev.* **2015**, *44*, 1974−2018.
(50) Wohlgemuth, M.; Yufa, N.; Hoffman, J.; Thomas, E. L. Triply Periodic Bicontinuous Cubic Microdomain Morphologies by Symmetries. *Macromolecules* **2001**, *34*, 6083−6089.
(51) Gotrik, K. W.; Hannon, A. F.; Son, J. G.; Keller, B.; Alexander-Katz, A.; Ross, C. A. Morphology Control in Block Copolymer Films Using Mixed Solvent Vapors. *ACS Nano* **2012**, *6*, 8052−8059.
(52) Wang, X. B.; Lo, T. Y.; Hsueh, H. Y.; Ho, R. M. Double and Single Network Phases in Polystyrene-*block*-poly(L-lactide) Diblock Copolymers. *Macromolecules* **2013**, *46*, 2997−3004.

DOI: 10.1021/acsami.5b03977
ACS Appl. Mater. Interfaces 2015, 7, 16536−16547